ISSN 0036-0244, Russian Journal of Physical Chemistry A, 2017, Vol. 91, No. 5, pp. 951–956. © Pleiades Publishing, Ltd., 2017.

PHYSICAL CHEMISTRY
OF NANOCLUSTERS AND NANOMATERIALS

Superparamagnetic and Ferromagnetic Behavior of $ZnFe_2O_4$ Nanoparticles Synthesized by Microwave-Assisted Hydrothermal Method[1]

Anukorn Phuruangrat[a,*], Wachiraporn Maisang[b], Thirawit Phonkhokkong[b], Somchai Thongtem[b,], and Titipun Thongtem[c,d]**

[a] *Department of Materials Science and Technology, Faculty of Science, Prince of Songkla University, Hat Yai, Songkhla 90112, Thailand*

[b] *Department of Physics and Materials Science, Faculty of Science, Chiang Mai University, Chiang Mai 50200, Thailand*

[c] *Department of Chemistry, Faculty of Science, Chiang Mai University, Chiang Mai 50200, Thailand*

[d] *Materials Science Research Center, Faculty of Science, Chiang Mai University, Chiang Mai 50200, Thailand*

**e-mail: phuruangrat@hotmail.com*

***e-mail: schthongtem@yahoo.com*

Received November 22, 2015

Abstract—Zinc ferrite ($ZnFe_2O_4$) nanoparticles were successfully synthesized from $Zn(NO_3)_2 \cdot 6H_2O$ and $Fe(NO_3)_3 \cdot 9H_2O$ by microwave hydrothermal method at 150°C for 1 h. Cubic $ZnFe_2O_4$ with particle size below 7 nm was formed in the solution at pH ≥ 6. The crystallinity and particle size of $ZnFe_2O_4$ nanoparticles were increased after calcination. The effects of pH of the precursor solution and calcination on the particle size and crystallinity of the particles were studied. At room temperature the products show superparamagnetic and ferromagnetic properties, determined by their size. The formation mechanism of $ZnFe_2O_4$ was also discussed according to the experimental results.

Keywords: zinc ferrite, magnetic properties, microwave-assisted hydrothermal method

DOI: 10.1134/S003602441705003X

1. INTRODUCTION

Metal ferrites (MFe_2O_4, M = Zn, Co, Ni, Cd) are among the most important magnetic materials and have many applications in electronic devices, information storage, magnetic resonance imaging (MRI), drug-delivery technology, catalysis and gas-sensing materials [1–3]. In recent years, zinc ferrite ($ZnFe_2O_4$) nanoparticles attract much attention due to their potential applications in gas sensors, adsorbents for hot-gas desulfurization, enzymatic biosensors and semiconductor photocatalysts [4–7]. $ZnFe_2O_4$ has normal spinel structure and has been intensively investigated [5, 8, 9]. Zn^{2+} and Fe^{3+} ions occupy the tetrahedral A and octahedral B sites of the spinel structure, respectively [8–10]. However, $ZnFe_2O_4$ is an antiferromagnetic material with the Néel temperature of ~10 K [8, 11, 12]. The magnetic properties of $ZnFe_2O_4$ significantly changed when its particle size was decreased to nanometer scale due to the inversion of Zn^{2+} and Fe^{3+} ions in B and A-sites [9, 12].

There are several methods used to synthesize $ZnFe_2O_4$ nanoparticles: hydrothermal reaction [2, 13], pyrolysis [5, 14], thermal decomposition [6, 8], electrospinning [7], co-precipitation [9, 15, 16] and solid state reaction [10, 11]. Moreover, they are rather time-consuming and may be complicated by formation of undesired phases. To solve such problems, another method for the preparation of $ZnFe_2O_4$ nanoparticles was developed. Microwave hydrothermal (MH) method was selected because it provide rapid heating, faster kinetics and low reaction temperature compared to conventional methods [4, 17, 18].

In the present work MH method was used to synthesize $ZnFe_2O_4$ nanoparticles with and without subsequent calcination at high temperature. Phase composition, morphology and magnetic properties of the prepared materials were investigated and discussed, along with proposed reaction mechanism and effect of pH.

2. EXPERIMENTAL

All reagents such as zinc nitrate hexahydrate ($Zn(NO_3)_2 \cdot 6H_2O$, 98%), iron nitrate nonahydrate ($Fe(NO_3)_3 \cdot 9H_2O$, ≥98%) and sodium hydroxide

[1] The article is published in the original.

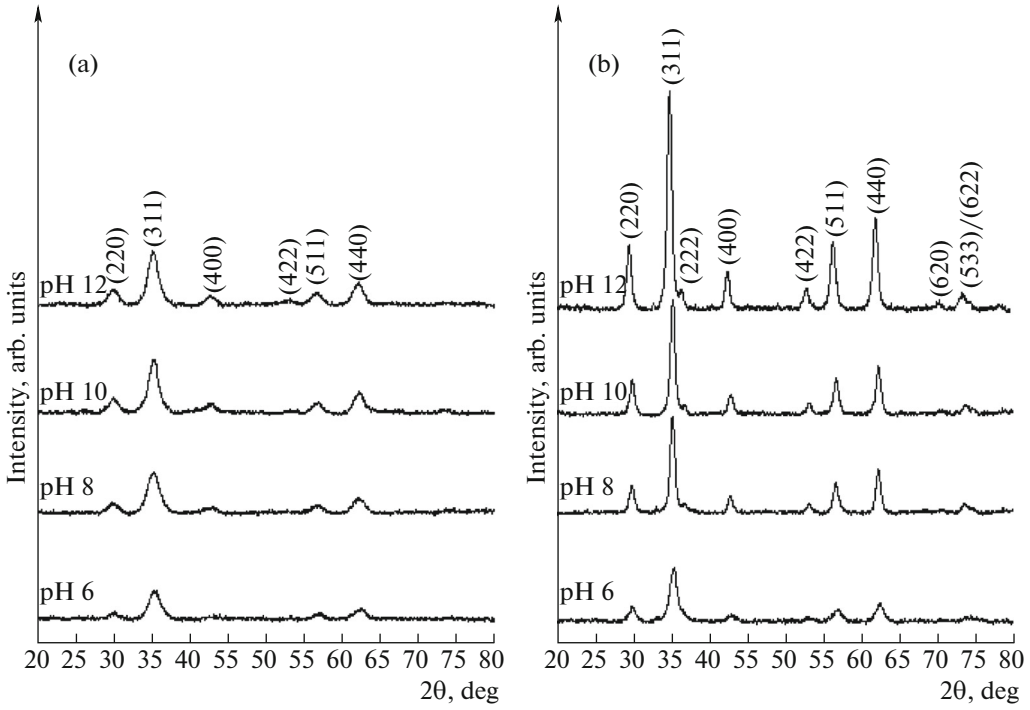

Fig. 1. XRD patterns of $ZnFe_2O_4$ samples synthesized at pH 6, 8, 10, and 12 by microwave-assisted hydrothermal method at 150°C for 1 h (a) before and (b) after calcination at 450°C for 1 h.

(NaOH, ≥99.5%), all from Sigma-Aldrich, were used without further purification.

In a typical synthetic procedure, zinc nitrate hexahydrate (5 mmol) and iron nitrate nonahydrate (10 mmol) were dissolved in 40 mL of deionized water. Then pH of the solutions was adjusted to desired value with 3 M NaOH. The resultant solutions were loaded in 100 mL fluoropolymer-lined pressure vessels (TFM®), which were then sealed and microwave-heated using Mars-5 unit (CEM Corporation) at 300 W from room temperature to 150°C within 20 min, and held at this temperature for 1 h, and then cooled to room temperature. The products were collected and washed with deionized water and ethanol, dried, and calcined at 450°C for 1 h.

X-ray powder diffraction (XRD) patterns were measured on a M18XHF X-ray diffractometer (MAC Science Co.). Transmission electron microscopy (TEM) was carried out on a JEOL JEM-2010 instrument operating at 200 kV. The samples for TEM analysis were prepared by dropping the dispersed products in ethanol on carbon copper grids. Fourier transform infrared spectra were recorded on a Bruker Tensor 27 FTIR spectrometer using standard KBr pellets. Magnetic properties of the samples were measured on a Lake Shore VSM 7403 vibrating sample magnetometer at room temperature over the ±10000 Oe range.

3. RESULTS AND DISCUSSION

Figure 1 shows XRD patterns of the products synthesized at described conditions, with pH being adjusted to 6, 8, 10, or 12 by 3 M NaOH solution. The XRD patterns can be indexed to cubic $ZnFe_2O_4$ spinel structure (JCPDS no. 79-1150 [19]). The diffraction peaks at 2θ of 30.1°, 35.2°, 42.8°, 52.9°, 56.5°, and 62.1° can be ascribed to the (220), (311), (400), (422), (511), and (440) planes of the spinel structure. No peaks of other phases were detected, indicating that the products are very pure. The broadening of fraction peaks implies the nanoscale size and low crystallinity of $ZnFe_2O_4$ particles. To improve their crystallinity, the products were calcined at 450°C for 1 h. The XRD patterns were still corresponding to the cubic $ZnFe_2O_4$ spinel phase. The $ZnFe_2O_4$ products remained as nanoparticles. The diffraction patterns became shaper and stronger, showing higher crystallinity of the calcined samples.

The approximate crystallite sizes of $ZnFe_2O_4$ samples before and after calcination were calculated from X-ray diffraction of the (311) plane using Scherrer formula:

$$B = \frac{\lambda k}{L\cos\theta}, \quad (1)$$

where λ is the wavelength of the CuK_α radiation, θ is the diffraction angle of the selected (311) peak, L is the full width at half maximum (FWHM) of the peak, B is the average crystallite size, and k is a constant [3, 20, 21]. The approximate crystallite sizes of $ZnFe_2O_4$ syn-

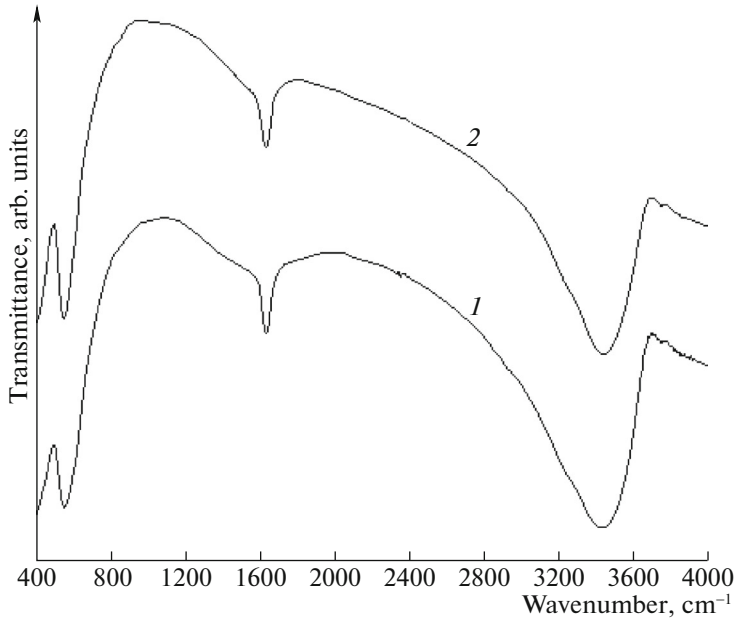

Fig. 2. FTIR spectra of $ZnFe_2O_4$ samples synthesized at pH 12 by microwave-assisted hydrothermal method at 150°C for 1 h (*1*) before and (*2*) after calcination at 450°C for 1 h.

thesized by microwave-hydrothermal method at pH 6, 8, 10, and 12 are 6.28, 7.48, 13.18, and 19.06 nm, respectively. For calcined materials, these sizes are 7.77, 12.85, 18.79, and 25.82 nm.

Figure 2 shows the FTIR spectra of $ZnFe_2O_4$ synthesized at pH 12 before and after calcination. IR spectroscopy is useful to detect the possible presence of residual species such as $Zn(OH)_x^{2-x}$ ($x = 2–4$) and $Fe(OH)_3$ in the main product. The broad band at 3375 cm^{-1} was believed to be associated with the OH stretching of adsorbed water molecules and hydroxyl groups on the surface of $ZnFe_2O_4$ nanoparticles [15, 16]. Additionally, the band at 1625 cm^{-1} was assigned to the bending vibration of water molecules. After calcination at 450°C for 1 h, the vibration band at 1362 cm^{-1} was no longer detected and the broad band at 3375 cm^{-1} was weakened. These results suggest that the calcination process can remove most of the surface hydroxyl groups and adsorbed water from the nanoparticles. Other bands at 553 and 400 cm^{-1} were assigned to intrinsic stretching vibration of Fe–O and Zn–O bonds at tetrahedral and octahedral sites of the $ZnFe_2O_4$ nanoparticles [3, 6, 9, 16].

TEM images and SAED patterns of the $ZnFe_2O_4$ particles synthesized by the MH method at different pH values before and after calcination are shown in Fig. 3. The products before calcination show cluster islands of nanoparticles with sizes below 10 nm. The particle sizes of $ZnFe_2O_4$ increased with increase of pH of the initial solutions. Their real sizes (Fig. 4) were counted for up to 300 particles. The average particle sizes and their standard deviations are 3.48 ± 0.51, 3.75 ± 0.53, 4.47 ± 0.59, and 5.76 ± 0.76 nm for the samples prepared at pH of 6, 8, 10, and 12, respectively. The same trend was observed for the particle sizes calculated by Scherrer formula. So, it can be concluded that pH of the precursor solutions determines the size of particles formed.

The SAED patterns of the particles before calcination showed diffuse and hollow rings, corresponding to very low crystallinity. This is in accordance with XRD data. The SAED patterns were indexed to (111), (220), (311), (222), (400), (422), (511), and (440) planes. Upon calcination of the samples at high temperature, the TEM images show narrow size distribution of spherical $ZnFe_2O_4$ nanoparticles. Their SAED patterns appear as bright spots of fully concentric rings, implying that the crystallinity of the particles had improved. These patterns can be indexed to the same planes of spinel structure. The size distributions for $ZnFe_2O_4$ particles before and after calcination can be fitted to normal distribution curves. The particle sizes of $ZnFe_2O_4$ increased with increase of pH of the precursor solutions. Their sizes also enlarged after calcination as well. These results are summarized in Table 1.

The formation of $ZnFe_2O_4$ nanoparticles by microwave-assisted hydrothermal method can be explained as follows. When iron and zinc nitrates were dissolved in water, pH of the resulting solution was 1.24. After addition of NaOH until pH 2–6, the freshly precipitated $Zn(OH)_2$ and $Fe(OH)_3$ formed directly from metallic salts. Subsequently, the solutions were heated by MH method at 150°C for 1 h, brown hydroxides

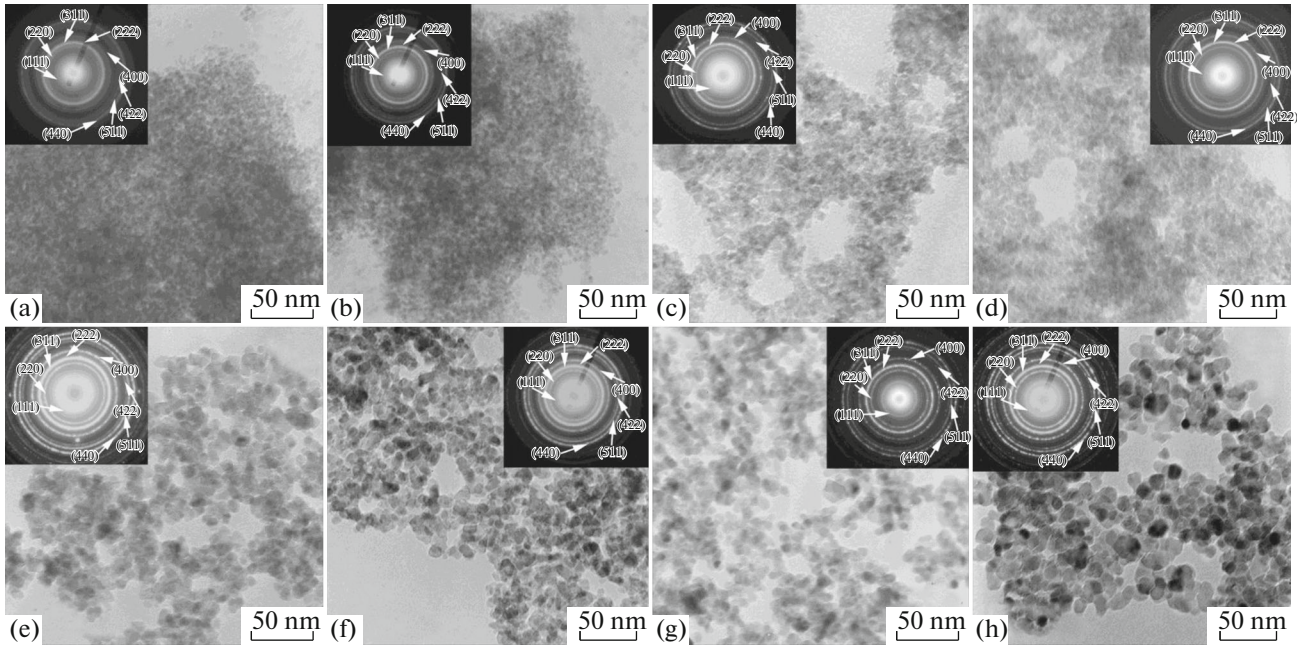

Fig. 3. TEM images and SAED patterns of $ZnFe_2O_4$ nanocrystals synthesized at pH (a, e) 6, (b, f) 8, (c, g) 10, and (d, h) 12 by microwave-assisted hydrothermal method at 150°C for 1 h (a–d) before and (e–h) after calcination at 450°C for 1 h.

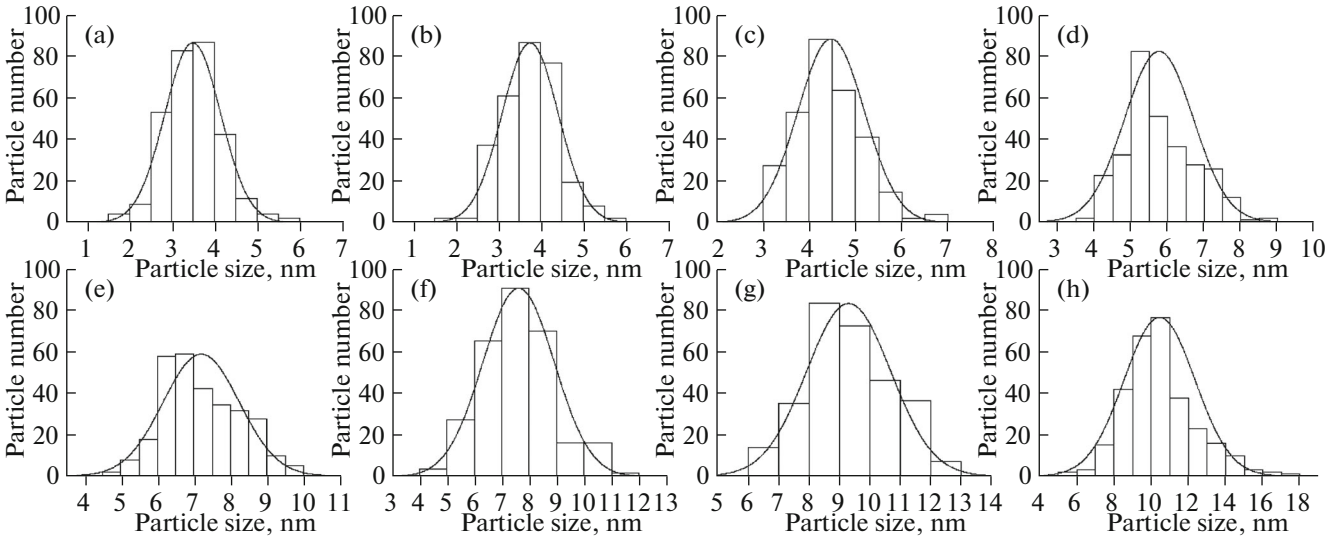

Fig. 4. Particle-size distributions of $ZnFe_2O_4$ nanocrystals synthesized at pH (a, e) 6, (b, f) 8, (c, g) 10, and (d, h) 12 by microwave-assisted hydrothermal method at 150°C for 1 h (a–d) before and (e–h) after calcination at 450°C for 1 h.

precipitated. The XRD patterns of the products formed at pH 2, 4, 5, and 6 are shown in Fig. 5. Products formed at initial pH 2 and 4 can be indentified as pure Fe_2O_3 phase (JCPDS no. 01-1053 [19]). At pH 5, the major $ZnFe_2O_4$ and minor Fe_2O_3 phases were detected. At pH 6, no Fe_2O_3 can be detected as impurity. It can be concluded that the appropriate condition for the formation of $ZnFe_2O_4$ nanoparticles is pH ≥ 6. Under microwave heating, the precipitated hydroxides were decomposed by microwave heating at high pressure to form oxide. The reaction mechanism for the formation of $ZnFe_2O_4$ nanocrystals during the MH synthesis can be explained as follows

$$Zn^{2+} + 2OH^- \rightarrow Zn(OH)_2, \quad (2)$$

$$Fe^{3+} + 3OH^- \rightarrow Fe(OH)_3, \quad (3)$$

$$Zn(OH)_2 + 2Fe(OH)_3 \rightarrow ZnFe_2O_4 + 4H_2O. \quad (4)$$

Table 1. Particle sizes of $ZnFe_2O_4$ nanoparticles obtained from TEM images

Solution pH	Particle size, nm	
	before calcination	after calcination
6	3.48 ± 0.51	7.20 ± 1.01
8	3.75 ± 0.53	7.61 ± 0.86
10	4.47 ± 0.59	9.30 ± 1.11
12	5.76 ± 0.76	10.44 ± 1.46

Table 2. Magnetic properties of $ZnFe_2O_4$ samples

Sample	Coercivity, Oe	Saturation magnetization, emu/g
pH 6, non-calcined	8.9042	19.4800
pH 12, non-calcined	6.7330	8.9516
pH 6, calcined	6.5847	4.6493
pH 12, calcined	5.3201	3.9095

Figure 6 shows magnetization at room temperature of $ZnFe_2O_4$ materials synthesized from the precursor solutions with pH 6 and 12 before and after calcination (Table 2). It should be noted that the $ZnFe_2O_4$ synthesized at pH 12 without calcination, and both calcined samples possess superparamagnetic properties with very low coercivity. This was attributed to an increased disorder of the magnetic moment orientation in the A and B sites. Moreover, only the $ZnFe_2O_4$ sample prepared at pH 6 without calcination shows ferromagnetic behavior with a saturation magnetization (M_S) of 19.48 emu/g. The magnetization values of all samples are summarized in Table 2. The saturation magnetization is decreased with increase of the particle size. The sample prepared at pH 6 has the highest saturation value, while calcined sample prepared at pH 12 has the lowest one. Lowering of the saturation magnetization is due to the presence of dead layer on the particle surfaces and tilted spins by small angles about their axes rather than being exactly co-parallel (spin canting). When particle sizes increase, the surface areas and the number of atoms on the surfaces decrease. Thus the saturation magnetization is lowered [2, 3, 6].

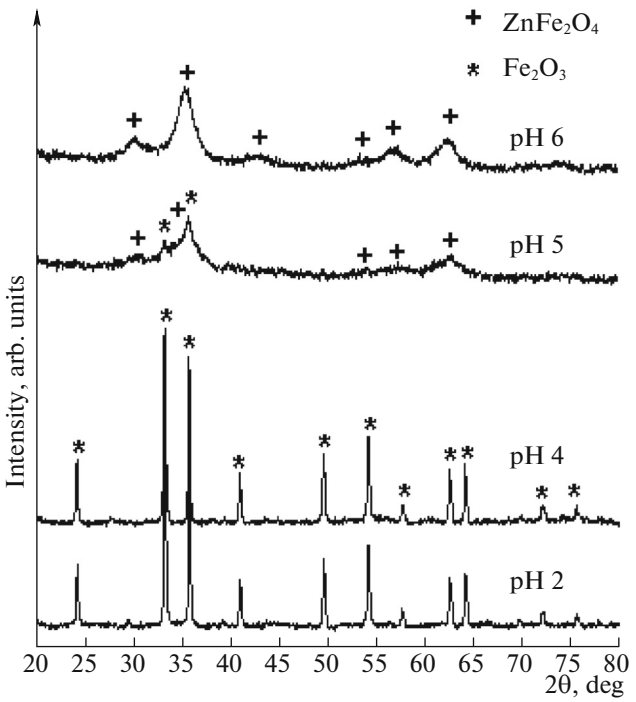

Fig. 5. XRD patterns of the products synthesized at pH 2, 4, 5, and 6 by microwave-assisted hydrothermal method at 150°C for 1 h.

4. CONCLUSIONS

In summary, well crystallized $ZnFe_2O_4$ nanoparticles were successfully synthesized in the solutions containing $Zn(NO_3)_2$ and $Fe(NO_3)_3$ with the pH of 6–12 by microwave-assisted hydrothermal method at 150°C for 1 h, followed by calcination at 450°C for 1 h. pH of the precursor solutions and calcination both affect the crystallinity and particle size of prepared $ZnFe_2O_4$ nanoparticles. The saturation magnetization of $ZnFe_2O_4$ nanocrystal synthesized at the pH of 6 by microwave-hydrothermal reaction at 150°C for 1 h was 19.48 emu/g.

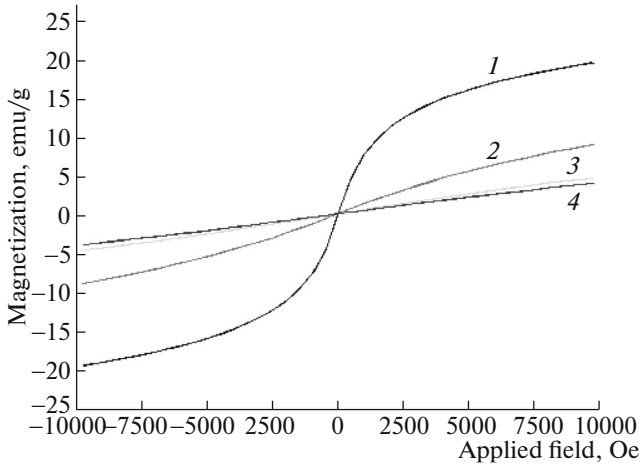

Fig. 6. Magnetic properties of $ZnFe_2O_4$ nanocrystals synthesized at pH 6 (*1*) and 12 (*2*) by microwave-assisted hydrothermal method at 150°C for 1 h and followed by calcination at 450°C for 1 h (*3* and *4*, respectively).

ACKNOWLEDGMENTS

We wish to thank Thailand's Office of the Higher Education Commission for financial support through the National Research University (NRU) Project for Chiang Mai University and Thailand Research Fund (TRF) through the contact IRG5780013.

REFERENCES

1. Z. Li, X. Lai, H. Wang, D. Mao, C. Xing, and D. Wang, J. Phys. Chem. C **113**, 2792 (2009).
2. S. H. Yu, T. Fujino, and M. Yoshimura, J. Magn. Magn. Mater. **256**, 420 (2003).
3. Y. Köseoğlu, A. Baykal, M. S. Toprak, F. Gğözüak, A. C. Başaran, and B. Aktas, J. Alloy Compd. **462**, 290 (2008).
4. S. W. Cao, Y. J. Zhu, G. F. Cheng, and Y. H. Huang, J. Hazard. Mater. **171**, 431 (2009).
5. G. Zhang, C. Li, F. Cheng, and J. Chen, Sens. Actuators B **120**, 403 (2007).
6. M. Wang, Z. Ai, and L. Zhang, J. Phys. Chem. C **112**, 13163 (2008).
7. M. G. Zhao, S. Fan, J. Liang, Y. Liun, Y. Li, J. Chen, and S. Chen, Ceram. Int. **41**, 40400 (2015).
8. C. Upadhyay, H. C. Verma, V. Sathe, and A. V. Pimpale, J. Magn. Magn. Mater. **312**, 271 (2007).
9. O. V. Yelenich, S. O. Solopan, T. V. Kolodiazhnyi, V. V. Dzyublyuk, A. I. Tovstolytkin, and A. G. Belous, Mater. Chem. Phys. **146**, 129 (2014).
10. F. Li, H. Wang, L. Wang, and J. Wang, J. Magn. Magn. Mater. **309**, 295 (2007).
11. S. Ozcan, B. Kaynar, M. M. Can, and T. Fi[dotless]rat, Mater. Sci. Eng. B **121**, 278 (2005).
12. J. Li, A. Wang, Y. Lin, X. Liu, J. Fu, and L. Lin, J. Magn. Magn. Mater. **330**, 96 (2013).
13. X. Chu, D. Jiang, and C. Zheng, Mater. Sci. Eng. B **129**, 150 (2006).
14. A. Sutkaa, J. Zavickis, G. Mezinskis, D. Jakovlevs, and J. Barloti, Sens. Actuators B **176**, 330 (2013).
15. J. Shen, G. Ma, J. Zhang, W. Quan, and L. Li, Appl. Surf. Sci. **359**, 455 (2015).
16. A. Shanmugavani, R. Kalai Selvan, Samar Layek, and C. Sanjeeviraja, J. Magn. Magn. Mater. **354**, 363 (2014).
17. D. Palma-Ramírez, M. A. Domínguez-Crespo, A. M. Torres-Huerta, H. Dorantes-Rosales, E. Ramírez-Meneses, and E. Rodríguez, J. Alloy Compd. **643**, S209 (2015).
18. K. Ocakoglu, Sh. A. Mansour, S. Yildirimcan, A. A. Al-Ghamdi, F. El-Tantawy, and F. Yakuphanoglu, Spectrochim. Acta A **148**, 362 (2015).
19. *Powder Diffraction File 79-1150* (JCPDS Int. Centre Diffraction Data, USA, 2001).
20. B. Rajesh Kumar and T. Subba Rao, Dig. J. Nanomater. Bios. **6**, 1281 (2011).
21. A. Phuruangrat, S. Thongtem, T. Thongtem, and B. Kuntalue, Dig. J. Nanomater. Bios. **7**, 1413 (2012).